Strategies for Mitigation of Hydrogen Environment Assisted Cracking of High Strength Steels

John R. Scully, Beth A. Kehler, Yongwon Lee and Richard P. Gangloff

20060713052

STRATEGIES FOR MITIGATION OF HYDROGEN ENVIRONMENT ASSISTED CRACKING OF HIGH STRENGTH STEELS

ABSTRACT

Modern ultra high strength alloy steels (UHSS) have been developed with outstanding combinations of strength and fracture toughness. Such steels are characterized by high purity and nanoscale strengthening clusters/coherent precipitates in a complex precipitation hardened, martensitic microstructure. However, the performance of such steels is degraded dramatically by internal hydrogen embrittlement (IHE) and hydrogen environment embrittlement (HEE). Thus, the development of an UHSS that is immune to hydrogen embrittlement is of seminal importance. The issues that hinder understanding of IHE/HEE center on the capability to first understand fracture process zone damage mechanisms, and second to quantify and ultimately predict crack tip hydrogen concentrations relative to critical concentrations that trigger fracture. Mitigation of the hydrogen-cracking resistance of modern UHSS requires reduction in hydrogen uptake and/or modification of critical hydrogen concentrations for a given material by improving the intrinsic tolerance to dissolved and trapped hydrogen. Strategies for controlling and/or mitigating HEE and IHE of UHSS include control of intrinsic intergranular susceptibility governed by hydrogen-segregated impurity interactions and metallurgical alteration of H trap states. Another strategy is to exploit the strong electrochemical potential dependency of HEE cracking by using tailored cathodic protection schemes. Lastly, coatings can be designed to release ions that reduce H production and/or block H uptake at crack tips. A combination of a responsive coating that provides a tailored-low level of cathodic protection and active corrosion inhibition, as well as control of metallurgical purity and H trap states, provides a necessary-couple strategy to mitigate HEE of modern high strength steels.

INTRODUCTION

Ultrahigh-strength steel (UHSS) is susceptible to severe internal hydrogen embrittlement (IHE), as well as hydrogen-environment embrittlement (HEE) [1-24]. In martensitic steels such as AISI 4340, this time-dependent subcritical cracking is typically intergranular (IG) along prior-

austenite grain boundaries, at apparent threshold stress-intensity (K_{TH}) levels approaching 10 MPa$\sqrt{m}$, and crack growth rates (da/dt) up to 10^4 µm/s [10,11,16]. K_{TH} for IG IHE and HEE decreases, and da/dt increases, with increasing σ_{YS} [2,10,13,14], dissolved-H concentration [2,6,10,19,23,24], and impurity content [1,3,4,18]. The da/dt value is directly proportional to the trap-sensitive effective diffusivity of H (D_H) for IHE and HEE in a wide range of high-strength alloys, but the critical distance ahead of the crack tip where H damage nucleates differs for IHE versus HEE due to different crack tip H distributions. Hydrogen diffusion about the crack tip limits the rate of such cracking, however, surface reaction kinetics can dominate rates of HEE for weak H-producing environments and high H-diffusivity alloys [11].

The mechanism for IG hydrogen cracking likely involves reduced grain boundary cohesion due to segregated H and impurities such as S, P, Sb, or Sn [3,18-20]. Thus, modern UHSS may resist IG hydrogen embrittlement through composition control. For example, UHSS AerMet 100 is produced by double-vacuum melting to yield ultra-low S and P levels, and neither Mn nor Si is added. This processing leads to a material that is prone to only limited IG HEE in acids and near-neutral chloride solutions with cathodic polarization, certainly much less so than less-pure UHSS [25-33]. The susceptibility of AERMET 100 to IG IHE is not established. Olson speculated that IG hydrogen cracking is eliminated by rare-earth element additions that reduce grain-boundary impurity segregation in UHSS [34,35]. However, micromechanical models of grain boundary decohesion suggest that H trapping and high stress at a crack tip are sufficient to promote hydrogen embrittlement without a dominant impurity contribution [2,11,13,14,19,36]. For example, 18Ni maraging steels contain only trace levels of P, S, Si, and Mn, but are susceptible to severe IG IHE and HEE [6-8].

Time-dependent IHE and HEE can also occur along transgranular (TG) paths in high strength steels [7,12,14,22], including martensite interfaces [3,9,37,38] and cleavage planes [39-41]. Interface cracking may be governed by decohesion, and cleavage cracking may occur due to a reduction in the work of fracture, both traced to dissolved H [39]. Changing environmental variables and the predissolved-H content affect an IG to TG crack-path change, as illustrated by the effect of temperature on HEE of 18Ni Maraging steel [9] and H-partitioning modeling [42]. For moderate strength, high purity steels, it has been found that subcritical TG cracking occurs at K_{TH} levels higher than those for IG H cracking [3,4]. Substantial TG HEE was reported for peak-aged AERMET 100 at low K_{TH} levels [25-33]. This TG H-cracking mode is traced to the low

concentration of metalloid impurities segregated to prior austenite grain boundaries, to minimize intergranular cracking, coupled with substantial H accumulation by trapping at transgranular sites in the crack tip process zone [43,44]. Thomas and coworkers demonstrated that optimally aged AERMET 100 is susceptible to severe IHE at threshold stress intensity levels as low as 20 MPa√m and produced by diffusible H contents as low as 1 part-per-million by weight (wppm) [44]. Lee and coworkers found that K_{TH} can be reduced to less than 20 MPa√m by HEE in 0.6 M NaCl at both anodic and cathodic potentials [45]. Both IHE and HEE in AERMET 100 are transgranular, associated with cracking of the various interfaces associated with the martensitic microstructure [25,26,30-32,44].

The IHE situation involves a fixed total amount of internal hydrogen introduced by H precharging. The cause of the time-dependent TG IHE susceptibility of AERMET 100 is the high concentration of diffusible H ($C_{H,diff}$) provided by easily repartitioned reversible trapping at strengthening precipitates and other sites in the martensite, high crack-tip stresses, and a connected path for TG cracking. Such reversibly trapped hydrogen may repartition to the tensile hydrostatic stress field of sharp cracks [46,47]. IHE resistance of UHSS may be improved by controlling these factors. For example, alloy additions that may enhance cohesion (B, C, or N) could displace elements than enhance decohesion (P, S, or Sn) and consequently raise the critical H level required to induce interfacial decohesion [48,49]. Metallurgical alteration of H trap states provides another means to eliminate IHE and possibly HEE in UHSS. For instance, reduction in M_2C carbide interface coherence by aging/Cr in a Co/C-hardened martensitic alloy steel (i.e., Fe-13Co-10Ni-3Cr-1Mo-0.25C) can raise the H trap binding energy of this benign site to reduce H repartitioning to martensite interfaces at stressed crack tips [50-53]. Metallurgical trap site modification forces a redistribution of hydrogen that is partitioned between lattice sites and trapping sites so that the critical hydrogen level required to induce interfacial decohesion is not readily obtained at the same hydrogen fugacity used in precharging [53,54]. However, overaging to affect this change in AERMET 100 will result in some strength loss and more precipitated austenite at martensite lath interfaces. The role of this austenite in IHE is uncertain. Alternately, carbides retained after solution treatment of AERMET 100 appear to be strong H traps [46]. The volume fraction of such carbides can be increased by changes in solution-treatment temperature or steel composition [55]. $C_{H,diff}$ would be reduced by strong and homogeneously distributed trap states, and time-dependent TG IHE resistance would be improved. However, these carbides

likely degrade K_{IC} by promoting void sheeting. Trapped H exacerbates this microvoid damage. In addition, time-dependent IHE resistance may be improved if martensite interfaces could be altered to lower E_b associated with these fracture sites. This would lead to a reduction in the amount of H that is strongly trapped at these sites and available for embrittlement.

The cause of HEE is the establishment of a high $C_{H,diff}$ at the crack tip governed by chemical and electrochemical factors, as well as crack tip metallurgy. Unlike the IHE situation that involves a fixed amount of hydrogen in a closed system, a continuous supply of hydrogen at the crack tip presents a greater challenge to mitigation of TG HEE. Strategies for controlling and/or mitigating HEE include controlling the intrinsic intergranular susceptibility governed by hydrogen-segregated impurity interactions. It is also possible that lowering of the trap-sensitive effective hydrogen diffusion rate slows the transport of hydrogen from the crack tip to the fracture process zone so as to severely restrict HEE crack growth rates [56]. Another metallurgical feature that can be controlled in this class of steel is retained austenite [57], which may act to getter H or control H transport from the crack tip to the fracture process zone. An additional strategy is to understand and possibly exploit the strong electrochemical potential dependency of HEE cracking [7,25,30,45,58-62]. Degradation of fracture toughness is a strong function of applied electrochemical potential in marine environments. Tailored coating compositions can be utilized to produce a galvanic couple potential at an optimal level to retard H production and uptake at near-surface crack tips. Exploitation of the potential dependency can lead to lower rates of hydrogen production and ingress, thereby lowering the dissolved and segregated hydrogen concentration in the lattice [53,63,64]. Lastly, coating design to release ions that reduce H production and/or block H uptake at crack tips is a possibility. A recently synthesized amorphous Al-Co-Ce-Mo coating could possibly serve in this function [65,66]. Co, Mo, Ce dissolve from a homogeneous amorphous coating or from phases in a heat treated alloy. Mo dissolves as Mo^{6+} (MoO_4^{2-}) that passivates (as does Cr^{6+}) an acidic crack. Co^{2+} and Ce^{3+} ions that are insoluble in alkaline solution can be precipitated to reduce cathodic H reaction kinetics and H uptake. Distributed storage of ions proximate to random cracks, release on demand, and transport to critical-occluded sites are feasible.

In summary, the combination of a responsive coating that provides a tailored low level of cathodic protection and active corrosion inhibition as well as control of metallurgical purity and H trap states offers the opportunity to mitigate HEE of modern high strength steels. The

theoretical implications of each of these strategies are discussed below in the context of the potential dependency of AERMET 100 HEE in 0.6 M NaCl. Confirmatory experiments are in progress.

MATERIAL

A forged bar of AERMET 100 was austenitized at 885°C, quenched in liquid nitrogen and peak aged at 482°C for an optimal combination of toughness and strength [44,46,47]. The chemical composition and mechanical properties for the peak aged condition are summarized in Tables 1 and 2 and the details of the microstructure are well documented [57].

Table 1. Chemical Composition of AERMET 100 (Weight Percent)

Fe	Co	Ni	Cr	Mo	C	Ti	P	S	H
Bal	13.43	11.08	3.00	1.18	0.23	.009	.003	.0008	0.26

Table 2. Mechanical Properties of AERMET 100

HRC	σ_{YS} (MPa)	σ_{UTS} (MPa)	RA (pct)	Strain-Hardening Exponent (1/n)	E (GPa)	σ_0 (MPa)	K_{IC} (MPa$\sqrt{m}$)
54	1725	1965	65	0.03	194.4	1985	126(LR)

AERMET 100 was developed to provide plane strain fracture toughness (K_{IC}) in excess of 120 MPa$\sqrt{m}$, doubling that of older steels such as AISI 4340 and 300M, each at constant yield strength (σ_{YS}) of 1750 MPa [67,68]. This strength is produced by a homogeneous distribution of nanoscale coherent M_2C alloy carbides in a highly dislocated Fe-Ni lath martensite matrix [69,70]. The high K_{IC} of AERMET 100 is achieved by advanced melting to minimize S + P and inclusion contents, austenitization to control undissolved carbides and grain size, and aging to optimize austenite precipitates along martensite lath interfaces [34,35,55,67].

APPROACH

Single edge notch (SEN) specimens were machined with a width (W) of 10.2 mm and thickness (B) of 2.54 mm. All specimens were machined parallel lengthwise to the radial direction of the

bar. The notch was electrospark discharge machined to a notch depth of 110±10 μm and width of 65±15 μm. Specimens were fatigue precracked to a total crack depth of 200 μm in air at 10 Hz at constant maximum stress intensity of 11 MPa√m and constant stress ratio of 0.10. Each precracked specimen was loaded in a 340 mL cylindrical Plexiglas cell. Non-deaerated (i.e., natural aeration conditions) 0.6 M NaCl (pH 6.4) was circulated from a 10 L reservoir at 24 mL/min. Only the gauge length of the specimen was exposed in the solution. Experiments were run in potentiostatic mode with applied potentials ranging from -1.1 to -0.5 V_{SCE} at a constant actuator displacement rate of 0.046 mm/hr, producing an initially constant rising stress intensity at a rate of 2.5 MPa-m$^{1/2}$/hr. Throughout the test duration, specimen load, actuator displacement, time, and direct current potential drop (dcPD) values were recorded with an automated data acquisition system [45]. The crack length (a) was calculated from the dcPD using an established calibration for the SEN specimen [71] and was corrected based on post-test measurements. The threshold stress intensity (K_{TH}) above which the environment induces resolvable subcritical crack growth was calculated form a plot of load (P) and dcPD (V) *vs* actuator displacement (δ). This procedure is described in previous work by Thomas, et al. [44].

RESULTS AND DISCUSSION

Potential Dependency of K_{TH}

Results presented in Figure 1 show that there is a narrow window of applied potentials that dramatically reduces the otherwise severe susceptibility of AERMET 100 to HEE. The severe drop in K_{TH} at applied potentials outside the narrow window can be attributed to high levels of hydrogen production and entry at crack tips. Scanning electron micrographs of the fracture surfaces at cathodic and anodic applied potentials reveal that the low levels of K_{TH} are associated with transgranular cracking (Figure 1b, left side of micrograph and Figure 1c) that is unique compared to the normal microvoid fracture mode (Figure 1b, right side of micrograph) and equivalent to the morphology of IHE in this steel [44]. The very high K_{TH} in Figure 1a, approaching K_{IC}, reflects a major improvement in resistance to HEE. However, a limited amount (~30 μm) of very slow H-enhanced TG crack growth was produced for this applied

potential of –625 mV$_{SCE}$, perhaps at K < K$_{TH}$. This residual amount of stable H cracking, as well as the occurrence of similar slow H cracking at –700 mV$_{SCE}$ is under investigation.

Micromechanical Modeling

IHE has been modeled micromechanically to predict K$_{TH}$, which decreases with increasing H concentration in the FPZ [36]. A recent model of brittle cracking in the presence of crack tip plasticity in the form of specific dislocation–crack-tip interactions, predicts K$_{TH}$ for H-decohesion-based fracture relative to the crack-tip Griffith toughness for H-free cracking [72].

$$K_{TH} = \frac{1}{\beta'_{IHE}} \exp\left[\frac{\left(k_{IG} - \alpha C_{H\sigma,T}\right)^2}{\alpha'' \sigma_{YS}}\right]$$

(1)

In this formulation, the Griffith threshold stress intensity for hydrogen embrittlement (k_{IH}) equals (k_{IG} - $\alpha C_{H\sigma,T}$) where α is a coefficient in units of MPa√m/atom fraction H and $C_{H\sigma,T}$ is the concentration of H localized by both trapping and stress field occlusion at the embrittlement site. The term k_{IG} is the critical Griffith stress-intensity factor for cleavage fracture without H ($G_C \sim \gamma_S \sim k_{IG}^2/E$), E is the elastic modulus, and γ_S is the energy required to produce a unit crack surface. For the Fe-Si system, k_{IG} = 0.85 MPa√m and α = 0.5 MPa√m/atom fraction H [72]. The β' and α'' terms are constants determined by computer simulation of the dislocation structure about the crack tip. Gerberich reported good correlation between modeled and experimental measurements of K_{TH} vs H$_2$ pressure and temperature for HEE of UHSS using α'' = 2x10^{-4} MPa·m and β'_{IHE} = 0.2 (MPa√m)$^{-1}$ [72]. This model has been applied to AERMET 100 and yields reasonable agreement with experimental results as shown in Figure 2 [44]. However, it is important to note that K$_{TH}$ is defined as the threshold stress intensity (K$_{TH}$) above which the environment induces a defined level of resolvable subcritical crack growth. For HEE, this value is affected by loading rate and crack growth can occur at K<K$_{TH}$. However, the Gerberich model provides a means a predicting the effects of metallurgy and electrochemistry on HEE.

Effect of Cohesion Promoters/Decohesion Inhibitors That Alter Work of Fracture

Approaches to produce H-cracking resistant UHSS by improving the purity of prior-austenite grain boundaries are important in mitigating intergranular HEE but may not be sufficient [18,34,35,37,38,73]. McMahon argued that segregants such as P, S, Sn, and Sb are a requisite for IG cracking, because H alone cannot localize sufficiently in the FPZ to enable low-K_{TH} IHE or HEE [3,18]. A correlation showed that HEE is eliminated if a bulk-composition parameter Ψ (Ψ = Mn + Si/2 + P + S + 10^4 C_H in at.%) is less than about 0.5 at.% for moderate-strength steels of 800 MPa < σ_{YS} < 1400 MPa and tempered martensitic microstructures heated through the temper-embrittlement regime [3,18]. Severe IG IHE seen in AISI 4340 and 300M steels is consistent with a high value of Ψ. However, Ψ is essentially 0 for AERMET 100 and 18Ni maraging steels, but hydrogen cracking along TG sites is severe as indicated in Figure 1. Thus, one mitigation strategy would be to add cohesion promoters or remove decohesion promoters in order to effectively increase k_{IG} and/or alter α. However, modeling of k_{IG} shown in Figure 3 for AERMET 100 over a range of applied potentials suggests that either a cohesion promoter or removal of a decohesion impurity is beneficial but insufficient in mitigating HE in AERMET 100. Figure 3 shows that decreasing k_{IG} from 1.31 to 0.85 MPa-m$^{1/2}$ has the effect of reducing the maximum K_{TH}, $K_{TH,MAX}$. However, while $K_{TH,MAX}$ increases with increasing k_{IG}, predicted K_{TH} values remain low at elevated hydrogen concentrations such as achieved at highly positive and negative potentials. That is, increasing k_{IG} has little effect on increasing the potential range over which susceptibility to HEE is reduced.

Effect of Raising E_b of Source Trap Sites that supply H to the Crack Tip via Stress Activated Repartitioning

For the case of IHE, a fixed total amount of internal H may be partitioned between various trap states and the lattice. From thermodynamic consideration, lattice H concentration is enhanced from an unstressed level of C_L to a stress-affected $C_{H\sigma}$ depending on the magnitude of the crack tip hydrostatic stress, σ_H [74]. The following equation applies assuming dilute H concentration, negligible effect of dissolved H on elastic constants of the material, and no negative deviation

from the logarithmic proportionality between $C_{H\sigma}$ and σ_H [50,75].

$$C_{H\sigma} = C_L \exp\left(\frac{\sigma_H V_H}{RT}\right) \tag{2}$$

The H concentration at trap sites in the crack tip process zone is further enhanced to $C_{H\sigma,T}$, according to Equation (3) where $E_{b\text{-site}}$ represents the binding energy of the trap at the fracture site [14]:

$$C_{H\sigma,T} = C_{H\sigma} \exp\left(\frac{E_{b-site}}{RT}\right) = C_L \exp\left(\frac{E_{b-site} + \sigma_H V_H}{RT}\right) \tag{3}$$

Hydrogen repartitions from a reversible trap state ($E_{b\text{-source}}$) to the trap at the crack tip ($E_{b\text{-site}}$) if the stress field interaction energy, $\sigma_H V_H$, exceeds $E_{b\text{-Source}}$ for the supplying trap near the tensile hydrostatic stress field. The amount of crack tip H at the crack tip fracture site is governed by the sum of $\sigma_H V_H$ and $E_{b\text{-site}}$ where this binding energy is for the highest energy trap state in the stress field that provides the interconnected crack path. The extent of H repartitioning from reversible traps to the stress field at the crack tip is given by [76,77]:

$$P_\sigma = \frac{\exp\left[\sigma_H V_H \big/ RT\right]}{\exp\left[\sigma_H V_H \big/ RT\right] \; + \; \exp\left[E_{b-source} \big/ RT\right]} \tag{4}$$

where P_σ is the probability that H occupies a lattice site under the influence of the crack tip hydrostatic stress field vs occupation of reversible trap sites surrounding the crack tip. Figure 4 shows the probability that hydrogen will repartition from a reversible trap state to the crack tip for several values of σ_H. Classical continuum fracture mechanics suggests that σ_H is 2.5 σ_{YS} for a low strain hardening UHSS [2,78]. Analyses based on either a crack tip dislocation perspective [40,79,80], or strain gradient plasticity hardening included in the flow curve [80,81] suggest that σ_H may be as high as $8\sigma_{YS}$. For each case, and particularly for the higher crack tip stresses, there

is a significant driving force for H to repartition from a dominant low energy trap state ($E_{b\text{-source}}$) to the crack tip.

This source of H from reversible traps contributes to the high level of $C_{H\sigma}$ that can accumulate at martensite interfaces in the crack tip process zone (10^{14} C_L from Equation (3), assuming that $\sigma_H = 5$ σ_{YS}, and actually exceeding 100 wt pct assuming that C_L is of order 10^{-4} wppm), thus explaining the severe IHE produced in AERMET 100 at low $K_{TH} \sim 0.1$ K_{IC} [44]. Notably, this hydrogen embrittlement was eliminated by baking the H-charged specimen at 190°C for 24 hours, which effectively removed diffusible and weakly trapped hydrogen [47]. Heating at 190°C did not eliminate H from higher energy trap states. However, this strongly trapped H did not produce embrittlement because it did not repartition to the crack tip. The probability for H repartitioning to the crack tip is very low when H is present only in higher energy traps (see Figure 4).

This analysis suggests an approach to improve the IHE resistance of aged AERMET 100. The coherence of M_2C decreases and Cr/Mo clusters are eliminated by aging at temperatures above about 500°C [57]. The resulting precipitates should have higher H-binding energy typical of incoherent interfaces. The idea would be to raise E_b above 30 kJ/mol as suggested by Figure 4 to suppress repartitioning of trapped hydrogen from source traps to the crack tip. A similar approach could be based on reductions in M_2C coherence by alloy additions [69]. Alloy yield strength will also be somewhat reduced. These changes will tend to reduce H partitioning from the reversible trap sites at M_2C to the crack tip hydrostatic stress field. If the reduction is sufficiently large, then H damage will be reduced, especially in a closed system such as pre-charged steel [44]. Experiments are required to test this speculation and establish the balance between the tensile strength, fracture toughness and IHE resistance of AERMET 100. However, this strategy may be more effective for IHE where a finite amount of hydrogen is available, assuming the traps are saturable, than for HEE where the crack tip can provide a constant H source.

Effect of Reducing E_b of Trap Sites involved in Fracture

Small palladium alloying additions reduce the susceptibility to hydrogen-assisted cracking in certain steels (e.g., quenched and tempered AISI 4130 steel) [82-87]. K_{ISCC} in sustained load

tests is significantly improved [54,84]. The fracture surface is modified such that intergranular cracking is replaced by transgranular tearing and ductile microvoid formation [54,84,85] when 1 wt pct Pd is added to the martensitic alloy at both 745 MPa (110 ksi) [54,84] and 1170 MPa (170 ksi) [85] yield strength levels. Explanations for this benefit of Pd addition are summarized below. Submonolayer coverages of Pd were found at lath boundaries and MnS-ferrite interfaces [84,88]. Tritium autoradiography indicated the absence of tritium at MnS inclusions when complexed by segregated Pd [89]. The reported explanation was that interfacial segregation of Pd to lath boundaries and interphase interfaces, such as sulfide inclusions, promoted rejection of hydrogen from these otherwise strong trapping sites for hydrogen [63,84,85,88,89]. The explanation for the role of Pd at such a site is based upon theoretical calculations of the Pd-hydrogen binding energies for Pd when present as individual substitutional atoms in an iron host lattice [90,91]. The calculated interaction energy for such diatomic complexes, which is the sum of a physical interaction and an electronic interaction, is dominated by the electronic interaction for Pd in an Fe host lattice [90]. This interaction energy is positive (repulsive), meaning that hydrogen should be repelled from such an impurity site in a host lattice. The argument made to support this concept is that elements to the right of iron in the periodic table tend toward filled valence electron shells and are less likely to accept additional electrons from a screened interstitial proton in the lattice [90-93]. This implies that Pd repels hydrogen when present as a single atom in an iron lattice. Therefore, it was postulated that hydrogen was either repelled from Pd-rich solid-solid interfaces or the binding energy was lowered [85,88]. Alternatively, elements such as Ti, which are to the left of iron in the periodic table, have more valence band electron vacancies than Fe and tend to trap hydrogen reversibly (negative electronic interaction) when present as sole atoms in an Fe host lattice [90-93].

The predicted effect of a reduced binding energy on K_{TH} is shown in Figure 5. The model assumes that E_b of the site controlling fracture was 30 kJ/mol, which may be associated with dislocations in the martensitic microstructure [46]. This value was used to compute $C_{H\sigma,T}$ (and thus $C_{lattice}$) values for experimental K_{TH} values using Equation (1) and assuming $k_{IG} = 1.31$ MPa-m$^{1/2}$, $\alpha = 1$ MPa-m$^{1/2}$, $\beta' = 0.2$ (MPa-m$^{1/2}$)$^{-1}$, and $\alpha'' = 3 \times 10^{-4}$ MPa-m (as per Figure 3). Then reduced $C_{H\sigma,T}$ values for trap sites with $E_b < 30$ kJ/mol were computed using Equation (3) enabling the prediction of K_{TH} using Equation (1). Note that a reduced trap site binding energy

leads to a greater range of potentials over which there is reduced susceptibility to hydrogen embrittlement.

Possible benefits of electrochemical potential control

The threshold for HEE is substantially increased and growth rates decreased in a narrow window of applied electrode potential for UHSS susceptible to severe transgranular HEE as shown in Figure 1. Figure 6 replots the effect of applied potential on K_{TH} for AERMET 100 in 3.5% NaCl revealing the window of reduced susceptibility to HEE in comparison to the open circuit potentials of various coatings [65,94,95]. Such coatings could control the galvanic couple potential and thus, K_{TH} (see Figure 6).

Thus, this window can be exploited by manipulating the galvanic couple potential between the coating and the exposed area of UHSS. In the case of the Al-Co-Ce coating, a range of OCPs can be preselected based on alloy composition and metallurgy [65]. Additionally, the width of this window of reduced susceptibility can be manipulated through the other strategies discussed above. For example, Figure 5 shows the effect of applied potential on K_{TH} for $E_{b\text{-site}}$ ranging from 20 to 30 kJ/mol. A reduced trap site binding energy leads to a greater range of potentials over which there is reduced susceptibility to hydrogen embrittlement. Using both alloy modification to lower $E_{b\text{-site}}$ plus a coating for polarization into the regime of increased resistance to HEE offers a viable strategy to mitigate hydrogen embrittlement.
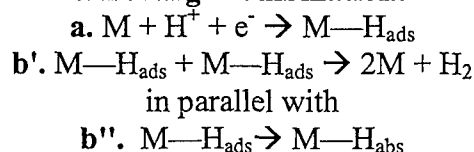
Effect of Inhibitors that Retard H uptake at Crack Tips

Galvanic coupling between a coating and an UHSS is unlikely to independently reduce the severity of HEE when potential windows of good HEE resistance are small. This is inferred from the severe IHE produced in AERMET 100 over a wide range of low to moderate diffusible hydrogen concentrations [44]. Results showed that there exists a critical diffusible hydrogen concentration of approximately 1 wppm above which K_{TH} is greatly reduced from K_{IC}. Thus, in order to mitigate HEE, the rate of hydrogen production and/or absorption must be reduced such that $C_{H,diff}$ remains below 1 wppm. Therefore, a coating must be multi-functional to act as a
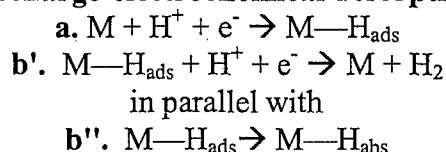
permeation barrier, to provide low levels of cathodic protection, and to act as a source for a supply of inhibiting ions in the vicinity of the crack tip.

Inhibitors function through several mechanisms including cathodic inhibition, anodic inhibition, H absorption inhibition, and enhanced H_2 recombinative desorption [96]. Indirect methods of inhibition include Cl^- absorption, pH buffers, and passivators. Two basic mechanisms for the hydrogen evolution reaction follow [97]:

Discharge-combination:
a. $M + H^+ + e^- \rightarrow M\text{—}H_{ads}$
b'. $M\text{—}H_{ads} + M\text{—}H_{ads} \rightarrow 2M + H_2$
in parallel with
b''. $M\text{—}H_{ads} \rightarrow M\text{—}H_{abs}$

Discharge-electrochemical desorption:
a. $M + H^+ + e^- \rightarrow M\text{—}H_{ads}$
b'. $M\text{—}H_{ads} + H^+ + e^- \rightarrow M + H_2$
in parallel with
b''. $M\text{—}H_{ads} \rightarrow M\text{—}H_{abs}$

Cathodic inhibitors act to reduce the overall rate of the hydrogen evolution reaction. Additionally, the recombination promoters work by increasing the rate of b', thereby reducing the rate of $H_{ads} \rightarrow H_{abs}$ via reaction b'' for a given overall reaction rate. Thus, cathodic inhibition and recombination promoters likely lead to a reduction in the amount of hydrogen absorbed into the metal [98]. Anodic inhibitors affect hydrogen absorption by inhibiting corrosion and thus inhibiting the hydrolysis reactions that create H^+ in an occluded solution, which can subsequently be reduced and absorbed at the crack tip [99]. Absorption inhibitors affect reaction kinetics by blocking absorption sites and thus reducing the effective surface area (i.e., inhibiting b'' above) or by promoting recombination of H atoms to produce H_2 (i.e., promoting b' above) [100]. Table 3 shows the traditional classes of H uptake inhibitors and examples.

Table 3. Inhibitor functions and examples [96,101,102].

Inhibitor function	Example compounds or species
Cathodic inhibitor	Polyphosphate, zinc, silicate
Anodic inhibitor	Chromate, nitrate, molybdate, cerate, orthophosphate, ferrocyanide
Chloride absorbers	Not determined
Acid Buffers	Borax, Sodium bicarbonate, etc.
Hydrogen entry inhibitors (not including passivators)	Bi, Pb, Zn, Noble metals, Various organic film formers
Recombination promoters	Ir, Pd, Pt

Thus, in the context of the Gerberich model, where K_{TH} decreases with increasing crack tip H concentration ($C_{\sigma H,T}$), inhibitors act by reducing the lattice H concentration, C_L, through direct or indirect reduction in reaction rates or absorption rates (see Figure 7), and subsequently, reducing $C_{\sigma H,T}$ (see Figure 3). It can be seen from Figure 7 that a 10-fold reduction in $C_{lattice}$ may be necessary to raise K_{TH} sufficiently at high anodic and cathodic potentials assuming $E_{b\text{-site}} = 30$ kJ/mol.

CLOSING STATEMENTS

Several strategies are possible for controlling and/or mitigating HEE and IHE of UHSS. These include controlling the intrinsic intergranular and transgranular susceptibility governed by hydrogen-segregated impurity interactions and metallurgical alteration of H trap states. Application of the Gerberich model to HEE of AERMET 100 showed that adding cohesion promoters or removing decohesion promoters (i.e., increasing k_{IG}) acts to increase $K_{TH,MAX}$, but does not substantially increase the potential range over which HEE susceptibility is reduced. Thus, this strategy may be more effective for IHE than for HEE. Application of the Gerberich model to alteration of H trap states (i.e., decreasing E_b of the trap site involved in fracture) shows an increased window of reduced susceptibility to HEE with decreasing $E_{b\text{-site}}$. Conversely, an increasing $E_{b\text{-source}}$ for sites that act as hydrogen sources was found to be beneficial as the probability of repartitioning to the FPZ decreases with increasing $E_{b\text{-source}}$. However, this strategy of increasing $E_{b\text{-source}}$ of the hydrogen sources may be more effective for IHE, assuming the source traps are saturable, than for HEE where there is a continuous supply of hydrogen. Lastly, coating design to release ions that reduce H production and/or block H uptake at crack tips is a possibility. Application of the Gerberich model shows that decreasing $C_{lattice}$ through inhibitor function leads to an increased window of reduced susceptibility to HEE for $E_{b\text{-site}} = 30$ kJ/mol. Thus, there are several strategies for controlling and/or mitigating HEE, but it is likely that a single strategy is not sufficient. Therefore, in order to exploit the outstanding combination of strength and fracture toughness in modern UHSS, a multi-pronged approach is recommended. A combination of a smart coating that provides a tailored-low level of cathodic protection and active corrosion inhibition as well as control of metallurgical purity and H trap states offers the opportunity to suppress HEE susceptibility of modern high strength steels.

REFERENCES

[1.] K. YOSHINO AND J. C.J. MCMAHON, METALL. TRANS. A, 1974. 5A: P. 363.

[2.] K.N. AKHURST AND T.J. BAKER, METALL. TRANS. A, 1981. 12A: P. 1059.

[3.] N. BANDYOPADHYAY, J. KAMEDA, AND J. C.J. MCMAHON, METALL. TRANS. A, 1983. 14A: P. 881.

[4.] S.K. BANERJI, H.C. FENG, AND J. C.J. MCMAHON, METALL. TRANS. A, 1978. 9A: P. 237.

[5.] C.F. BARTH AND E.A. STEIGERWALD, METALL. TRANS., 1970. 1: P. 3451.

[6.] D.P. DAUTOVICH AND S. FLOREEN, METALL. TRANS., 1973. 4: P. 2627.

[7.] D.P. DAUTOVICH AND S. FLOREEN, IN *STRESS CORROSION CRACKING AND HYDROGEN EMBRITTLEMENT OF IRON ALLOYS*, R.W.S.E. AL., EDITOR. 1977, NACE: HOUSTON, TX. P. 798.

[8.] R.P. GANGLOFF AND R.P. WEI, METALL. TRANS. A, 1977. 8A: P. 1043.

[9.] R.P. GANGLOFF AND R.P. WEI, IN *FRACTOGRAPHY IN FAILURE ANALYSIS, ASTM STP 645*, B.M. STRAUSS AND J. W.H. CULLEN, EDITORS. 1978, ASTM: WEST CONSHOHOCKEN, PA. P. 87.

[10.] R.P. GANGLOFF, IN *CORROSION PREVENTION AND CONTROL*, M. LEVY AND S. ISSEROW, EDITORS. 1986, UNISTED STATES ARMY MATERIALS TECHNOLOGY LABORATORY: WATERTOWN, MA. P. 64.

[11.] R.P. GANGLOFF, IN *HYDROGEN EFFECTS IN MATERIALS*, N.R. MOODY, ET AL., EDITORS. 2002, TMS: WARRENDALE, PA. P. 477.

[12.] M. GAO, M. LU, AND R.P. WEI, METALL. TRANS. A, 1984. 15A: P. 735.

[13.] W.W. GERBERICH, T. LIVNE, AND X. CHEN, IN *MODELING ENVIRONMENTAL EFFECTS ON CRACK GROWTH PROCESSES*, R.H. JONES AND W.W. GERBERICH, EDITORS. 1986, TMS: WARRENDALE, PA. P. 243.

[14.] W.W. GERBERICH, T. LIVNE, X.-F. CHEN, AND M. KACZOROWSKI, METALL. TRANS. A, 1988. 19A: P. 1319.

[15.] H.H. JOHNSON, J.G. MORELET, AND A.R. TROIANO, TRANS. TMS-AIME, 1958. 216: P. 528.

[16.] G.E. KERNS, M.T. WANG, AND R.W. STAEHLE, IN *STRESS CORROSION CRACKING AND HYDROGEN EMBRITTLEMENT OF IRON ALLOYS*, E.A. R.W. STAEHLE, EDITOR. 1977, NACE: HOUSTON, TX. P. 700.

[17.] P. MCINTYRE, IN *HYDROGEN DEGRADATION OF FERROUS ALLOYS*, R.A. ORIANI, J.P. HIRTH, AND M. SMIALOWSKI, EDITORS. 1985, NOYES PUBLICATIONS: PARK RIDGE, NJ. P. 763.

[18.] C.J. MCMAHON(JR.), ENG. FRACT. MECH., 2001. 68: P. 773.

[19.] R.A. ORIANI AND P.H. JOSEPHIC, ACTA METALL., 1974. 22: P. 1065.

[20.] R.A. ORIANI, CORROSION, 1987. 43: P. 390.

[21.] E.A. STEIGERWALD, F.W. SCHALLER, AND A.R. TROIANO, TRANS. TMS-AIME, 1960. 218: P. 832.

[22.] R.P. WEI AND M. GAO, IN *HYDROGEN DEGRADATION OF FERROUS ALLOYS*, R.P. ORIANI, J.P. HIRTH, AND M. SMIALOWSKI, EDITORS. 1985, NOYES PUBLICATIONS: PARK RIDGE, NJ. P. 579.

[23.] Y. YAMAGUCHI, H. NONAKA, AND K. YAMAKAWA, CORROSION, 1997. 53: P. 147.

[24.] K. YAMAKAWA, S. YONEZAWA, AND S. YOSHIZAWA. IN *INT. CONGR. ON METALLIC CORROSION*. 1984. TORONTO: NATIONAL RESEARCH COUNCIL.

[25.] E.U. LEE, H. SANDERS, AND B. SARKAR. IN *PROC. TRI-SERVICE CONF. ON CORROSION*. 2000. ABERDEEN, MD: ARMY RESEARCH LABORATORY.

[26.] G.N. VIGILANTE, J.H. UNDERWOOD, AND D. CRAYTON. IN *FATIGUE AND FRACTURE MECHANICS, PROC. 30TH NAT. SYMP.* 2000. WEST CONSHOHOCKEN, PA: ASTM INTERNATIONAL.

[27.] J. KOZOL AND C.E. NEU. 1992, NAVAL AIR WARFARE CENTER: WARMINSTER, PA.

[28.] A. OEHLERT AND A. ATRENS, MATER. FORUM, 1993. 17: P. 415.

[29.] A. OEHLERT AND A. ATRENS, J. MATER. SCI., 1998. 33: P. 775.

[30.] P.F. BUCKLEY, R. BROWN, G.H. GRAVES, E.U. LEE, C.E. NEU, AND J. KOZOL, IN *METALLIC MATERIALS FOR LIGHTWEIGHT APPLICATIONS, 40TH SAGAMORE ARMY MATERIALS RESEARCH CONF.*, M.G.H. WELLS, E.B. KULA, AND J.H. BEATTY, EDITORS. 1993, UNITED STATES ARMY LABORATORY COMMAND: WATERTOWN, MA. P. 377.

[31.] P. BUCKLEY, B. PLACZANKIS, J. BEATTY, AND R. BROWN. IN *CORROSION/94*. 1994. HOUSTON, TX: NACE.

[32.] E.U. LEE, METALL. TRANS. A, 1995. 26A: P. 1313.

[33.] D.S. MCDARMAID, BR. CORR. J., 1980. 15: P. 172.

[34.] G.B. OLSON, IN *INNOVATIONS IN ULTRAHIGH STRENGTH STEEL TECHNOLOGY, 34TH SAGAMORE ARMY MATERIALS RESERACH CONF.*, G.B. OLSON, M. ARZIN, AND E.S. WRIGHT, EDITORS. 1987, UNITED STATES ARMY LABORATORY COMMAND: WATERTOWN, MA. P. 549.

[35.] G.B. OLSON, ADV. MATER. PROCESSES, 1997. JULY: P. 72.

[36.] R.P. GANGLOFF, MATER. SCI. ENG., 1988. A103: P. 157.

[37.] J. KAMEDA AND J. C.J. MCMAHON, METALL. TRANS. A, 1983. 14A: P. 903.

[38.] Y. TAKEDA AND J. C.J. MCMAHON, METALL. TRANS. A, 1981. 12A: P. 1255.

[39.] J.F. KNOTT, IN *HYDROGEN EFFECTS IN MATERIALS*, A.W. THOMPSON AND N.R. MOODY, EDITORS. 1996, TMS: WARRENDALE, PA. P. 287.

[40.] X. CHEN AND W.W. GERBERICH, METALL. TRANS. A, 1991. 22A: P. 59.

[41.] M. GAO AND R.P. WEI, ACTA METALL., 1984. 32: P. 2115.

[42.] M. GAO AND R.P. WEI, METALL. TRANS. A, 1985. 16A: P. 2039.

[43.] R.P. GANGLOFF, IN *COMPREHENSIVE STRUCTURAL INTEGRITY*, I. MILNE, R.O. RITCHIE, AND B. KARIHALOO, EDITORS. 2003, ELSEVIER SCIENCE: NEW YORK, NY. P. 31.

[44.] R.L.S. THOMAS, J.R. SCULLY, AND R.P. GANGLOFF, METALL. MATER. TRANS. A, 2003. 34A: P. 327.

[45.] Y. LEE, B.A. KEHLER, R.P. GANGLOFF, AND J.R. SCULLY, *HYDROGEN ENVIRONMENT EMBRITTLEMENT OF AERMET 100*. 2005: CHARLOTTESVILLE, VA.

[46.] R.L.S. THOMAS, D. LI, R.P. GANGLOFF, AND J.R. SCULLY, METALL. MATER. TRANS. A, 2002. 33A: P. 1991.

[47.] D. LI, R.P. GANGLOFF, AND J.R. SCULLY, *HYDROGEN DIFFUSION AND TRAPPING BEHAVIOR IN ULTRAHIGH STRENGTH AERMET 100 STEEL*. 2002, UNIVERSITY OF VIRGINIA: CHARLOTTESVILLE, VA.

[48.] H.J. GRABKE, *CHEMISTRY AND PHYSICS OF FRACTURE*. 1987, BOSTON, MA: MARTINUS NIJHOFF PUBLISHERS/NATO SCIENTIFIC AFFAIRS. 388.

[49.] J.R. RICE AND J.S. WANG, MATER. SCI. ENG. A., 1989. A107: P. 23.

[50.] J.P. HIRTH, METALL. TRANS. A, 1980. 11A: P. 861.

[51.] I.M. BERNSTEIN AND G.M. PRESSOUYRE, IN *HYDROGEN DEGREDATION OF FERROUS ALLOYS*, R.A. ORIANI, J.P. HIRTH, AND M. SMIALOWSKI, EDITORS. 1985, NOYES PUBLICATIONS: PARK RIDGE, NJ. P. 641.

[52.] G.M. PRESSOUYRE AND I.M. BERNSTEIN, METALL. TRANS. A, 1978. 9A: P. 1571.

[53.] G.M. PRESSOUYRE, IN *CURRENT SOLUTIONS TO HYDROGEN PROBLEMS IN STEELS, PROC. 1ST INT. CONF.*, C.G. INTERRANTE AND G.M. PRESSOUYRE, EDITORS. 1982, ASM: METALS PARK, OH. P. 18.

[54.] B.E. WILDE, C.D. KIM, AND J. J.C. TURN, CORROSION, 1982. 38: P. 515.

[55.] C.J. KUEHMANN. 1994, NORTHWESTERN UNIVERSITY: EVANSTON, IL.

[56.] R.P. GANGLOFF. *DIFFUSION CONTROL OF HYDROGEN ENVIRONMENT EMBRITTLEMENT IN HIGH STRENGTH ALLOYS. IN HYDROGEN EFFECTS ON MATERIAL BEHAVIOR AND CORROSION DEFORMATION INTERACTIONS.* 2003. MORAN, WYOMING: TMS (THE MINERALS, METALS & MATERIALS SOCIETY).

[57.] R. AYER AND P.M. MACHMEIER, METALL. TRANS. A, 1993. 24A: P. 1943.

[58.] B.F. BROWN, *STRESS CORROSION CRACKING OF HIGH STRENGTH STEEL ALLOYS*, IN *THEORY OF SCC IN ALLOYS*, J.C. SCULLY, EDITOR. 1971, NATO SCIENTIFIC AFFARIS DIVISION: BRUSSELS. P. 186.

[59.] B.F. BROWN. IN *STRESS CORROSION CRACKING AND HYDROGEN EMBRITTLEMENT OF IRON ALLOYS.* 1977: NACE.

[60.] B.F. BROWN, C.T. FUJII, AND E.P. DALBERG, J. ELECTROCHEM. SOC., 1969. 116: P. 218.

[61.] G. SANDOZ, *HIGH STRENGTH STEELS*, IN *STRESS CORROSION CRACKING IN HIGH STRENGTH STEELS AND IN TITANIUM AND ALUMINUM ALLOYS*, B.F. BROWN, EDITOR. 1972, NAVAL RESEARCH LABORATORY: WASHINGTON, DC.

[62.] P.S. TYLER, M. LEVY, AND L. RAYMOND, CORROSION, 1991. 47: P. 82.

[63.] M. ZAMANZADEH, A. ALLAM, AND H.W. PICKERING, J. ELECTROCHEM. SOC., 1980. 127: P. 1688.

[64.] M. IINO, N. NOMURA, AND H. TAKEZAWA, IN *CURRENT SOLUTIONS TO HYDROGEN PROBLEMS IN STEELS, PROC. 1ST INT. CONF.*, C.G. INTERRANTE AND G.M. PRESSOUYRE, EDITORS. 1982, ASM: METALS PARK, OH. P. 159.

[65.] M.E. GOLDMAN, N. UNLU, G.J. SHIFLET, AND J.R. SCULLY, ELECTROCHEMICAL AND SOLID-STATE LETTERS, 2005. 8(2): P. B1.

[66.] M. JAKAB AND J.R. SCULLY, NATURE MATERIALS, 2005(4): P. 1.

[67.] W.M. GARRISON(JR.), J. MET., 1990. 46: P. 20.

[68.] R.M. HEMPHILL AND D.E. WERT, 5087415, CARPENTER TECHNOLOGY CORPORATION, READING, PA, 1992.

[69.] R. AYER AND P.M. MACHMEIER, METALL. TRANS. A, 1996. 27A: P. 2510.

[70.] C.H. YOO, H.M. LEE, J.W. CHAN, AND J.W. MORRIS, METALL. MATER. TRANS. A, 1996. 27A: P. 3466.

[71.] H.H. JOHNSON, MATERIALS RESEARCH & STANDARDS, 1965. 5(9): P. 442.

[72.] W.W. GERBERICH, P.G. MARSH, AND J.W. HOEHN, IN *HYDROGEN EFFECTS IN METALS.* 1996, TMS: WARRENDALE, PA. P. 539.

[73.] J.F. WATTON, G.B. OLSON, AND M. COHEN, IN *INNOVATIONS IN ULTRAHIGH STRENGTH STEEL TECHNOLOGY, 34TH SAGAMORE ARMY MATERIALS RESERACH CONF.*, G.B. OLSON, M. AZRIN, AND E.S. WRIGTH, EDITORS. 1987, UNITED STATES ARMY LABORATORY COMMAND: WATERTOWN, MA. P. 549.

[74.] R.A. ORIANI, IN *FUNDAMENTAL ASPECTS OF STRESS CORROSION CRACKING.* 1969, NACE: HOUSTON, TX. P. 32.

[75.] W.C. JOHNSON AND J.Y. HUH, METALL. MATER. TRANS. A, 2003. 34A(12): P. 2819.

[76.] T.Y. ZHANG, H. SHEU, AND J.E. HACK, SCRIPTA METALL. MATER., 1992. 27: P. 1605.

[77.] T.Y. ZHANG AND J.E. HACK, METALL. MATER. TRANS. A, 1999. 30A: P. 155.

[78.] T.L. ANDERSON, *FRACTURE MECHANICS: FUNDAMENTALS AND APPLICATIONS.* 2ND ED. 1995, BOCA RATON, FL: CRC PRESS. 117.

[79.] W.W. GERBERICH, R.A. ORIANI, M.-J. LI, X. CHEN, AND T. FOECKE, PHIL. MAG. A, 1991. 63: P. 363.

[80.] Y. WEI AND J.W. HUTCHINSON, J. MECH. PHYS. SOLIDS, 1997. 45: P. 1253.

[81.] H. JIANG, Y. HUANG, Z. ZHUANG, AND K.C. HWANG, J. MECH. PHYS. SOLIDS, 2001. 49(979-93).

[82.] U.P. LEVENKO, CERNAJI METALL., 1975. 10: P. 116.

[83.] V.I. ARKHAROV, T.T. MOROZ, I.A. NOVOKHATSKII, S.I. KHOKHLOVA, AND M.I. EREMIA, SOV. MATER. SCI., 1976. 12: P. 38.

[84.] J.B. LUMSDEN, B.E. WILDE, AND P.J. STOCKER, SCRIPTA METALL., 1983. 17: P. 971.

[85.] B.E. WILDE, I. CHATTORAJ, AND T.A. MOZHI, SCRIPTA METALL., 1987. 21: P. 1369.

[86.] J.R. SCULLY, M.J. CIESLAK, AND J.A.V.D. AVYLE, SCRIPTA METALL., 1994. 31(2): P. 125.

[87.] J.R. SCULLY, J.A.V.D. AVYLE, M.J. CIESLAK, J. A.D. ROMIG, AND C.R. HILLS, METALL. MATER. TRANS. A, 1991. 22A: P. 2429.

[88.] M.K. MILLER, S.S. BRENNER, AND M.G. BURKE, METALL. TRANS. A, 1987. 18A: P. 519.

[89.] T.D. LE AND B.E. WILDE. IN CURRENT SOLUTIONS TO HYDROGEN PROBLEMS IN STEELS, PROC. 1ST INT. CONF. 1982. METALS PRAK, OH: ASM.

[90.] A.I. SHIRLEY AND C.K. HALL, SCRIPTA METALL., 1983. 17: P. 1003.

[91.] H. KRONMULLER, B. HOHLER, H. SCHREYER, AND K. VETTER, PHIL. MAG. B, 1978. 37(5): P. 569.

[92.] G.M. PRESSOUYRE, METALL. TRANS. A, 1983. 14A: P. 2189.

[93.] G.M. PRESSOUYRE, METALL. TRANS. A, 1979. 10A: P. 1571.

[94.] H.P. HACK, METALS HANDBOOK. 1987, ASM: METALS PARK, OH. P. 234.

[95.] B.N. POPOV. 2005.

[96.] V.S. AGARWALA. MODIFICATION OF CRACK-TIP CHEMISTRY TO INHIBIT CORROSION AND STRESS CORROSION CRACKING IN HIGH-STRENGTH ALLOY. IN EMBRITTLEMENT BY THE LOCALIZED CRACK ENVIRONMENT. 1983. PHILADELPHIA, PA: THE METALLURGICAL SOCIETY/AIME.

[97.] P.K. SUBRAMANYAN, ELECTROCHEMICAL ASPECTS OF HYDROGEN IN METALS, IN COMPREHENSIVE TREATISE ON ELECTROCHEMISTRY, J.O.M. BOCKRIS, B.E. CONWAY, AND E. YEAGER, EDITORS. 1981, PLENUM: NY, NY. P. 411.

[98.] L. MAKSAEVA, A. MARSHAKOV, Y. MIKHAILOVSKY, AND V. POPOVA. IN CORROS. CONTROL LOW-COST RELIAB., PROC. - 12TH INT. CORROS. CONGR. 1993: NACE.

[99.] C.C. JUANG AND J.K. WU, CORROSION SCIENCE, 1994. 36(10): P. 1727.

[100.] L. VRACAR AND D.M. DRAZIC, J. ELECTROANAL. CHEM., 1992. 339: P. 269.

[101.] C.T. LYNCH, K.J. BHANASALI, AND P.A. PARRISH, INHIBITION OF CRACK PROPAGATION OF HIGH STRENGTH STEELS THROUGH SINGLE AND MULTI-FUNCTIONAL INHIBITORS, W. PATTERSON, EDITOR. 1976.

[102.] B.N. POPOV, G. ZHENG, AND R.E. WHITE, CORROSION, 1995. 51(6): P. 429.

a.
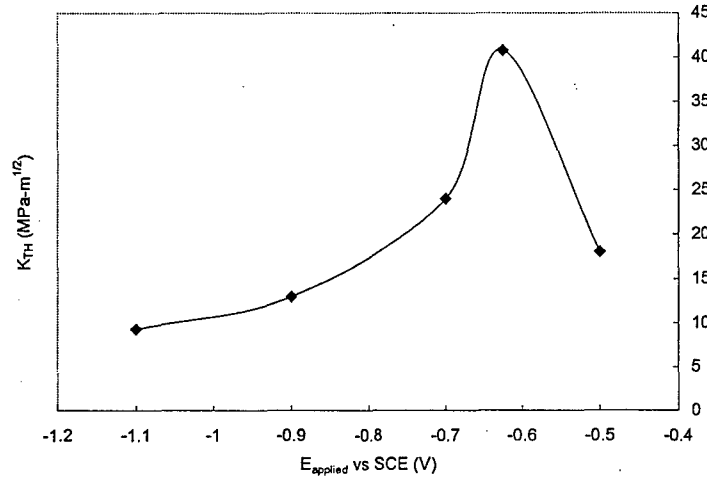
b.
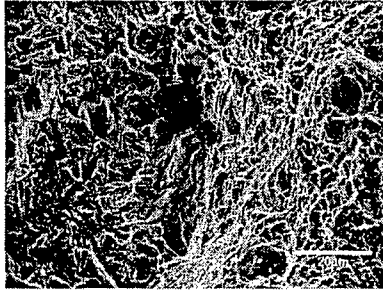
c.

Figure 1. a) K_{TH} versus applied potential for AERMET 100 in 0.6 M NaCl. b) and c) show scanning electron images of the fracture surfaces for applied potentials of -1.1 V_{SCE} and -0.5 V_{SCE}, respectively.
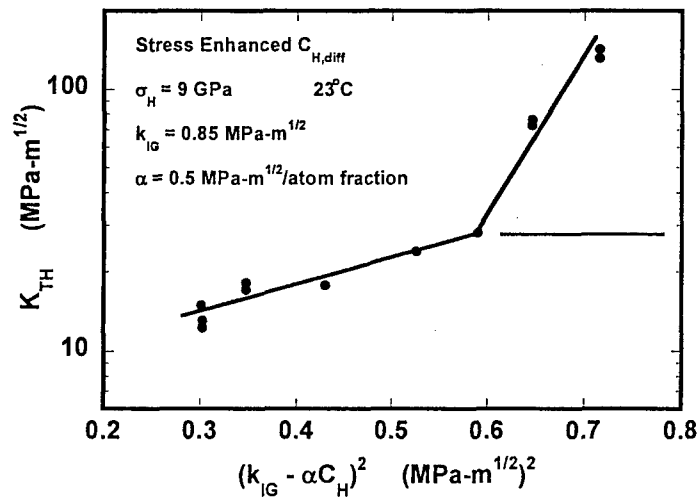

Figure 2. The measured (●) and model-predicted (—) effects of hydrostatic-stress enhanced H concentration on K_{TH} for IHE of AERMET 100. All measured K_{TH} values less than 30 MPa-$m^{1/2}$ relate to brittle-transgranular IHE and the associated regression line is $\log(K_{TH}) = 0.83 + 1.05 (k_{IG} - \alpha C_H)^2$ with $R^2 = 0.89$. Cracking at higher K_{TH} involved some MVC [44].
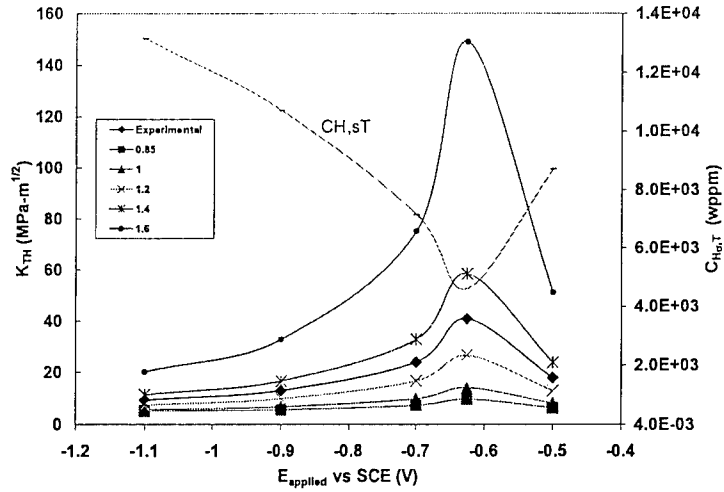
Figure 3. Predicted (dotted lines) and experimental ($\blacklozenge$) K_{TH} versus $E_{applied}$ for values of k_{IG} ranging from 0.85 to 1.6 MPa-m$^{1/2}$. $C_{H\sigma,T}$ values were calculated through Equation (1) using experimental K_{TH} values for AERMET 100 in 0.6 M NaCl and a k_{IG} of 1.31 MPa-m$^{1/2}$. This value of k_{IG} was chosen to correspond to approximately 0 wppm hydrogen at K_{IC}. A value of α = 1 MPa-m$^{1/2}$/ atom fraction H was chosen corresponding with $\beta' = 0.2$ (MPa-m$^{1/2}$)$^{-1}$ and $\alpha'' = 3 \times 10^{-4}$ MPa-m.
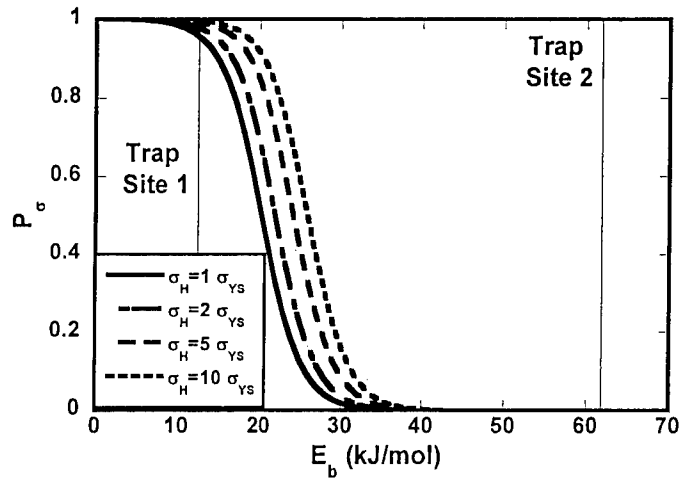

Figure 4. Probability of repartitioning to the FPZ given by Equation (4) at hydrostatic stresses ranging from σ_{YS} to 10 σ_{YS} for metallurgical trap sites with $E_b \leq 70$ kJ/mol. Also, shown are lines indicating AERMET 100 trap site 1, which is associated with coherent M$_2$C precipitates and trap site 2, which is associated with martensite interfaces, austenite grain boundaries, and mixed dislocation cores [47].
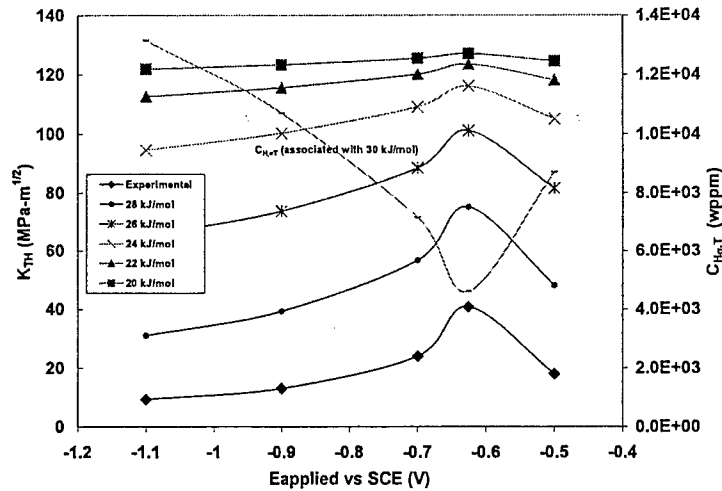
Figure 5. Predicted (dotted lines) and experimental (◆) K_{TH} versus $E_{applied}$ for trap site binding energies at the critical fracture site ($E_{b\text{-}site}$) ranging from 20 to 30 kJ/mol. A hydrostatic stress field, σ_H, of $5\sigma_{ys}$ is assumed.
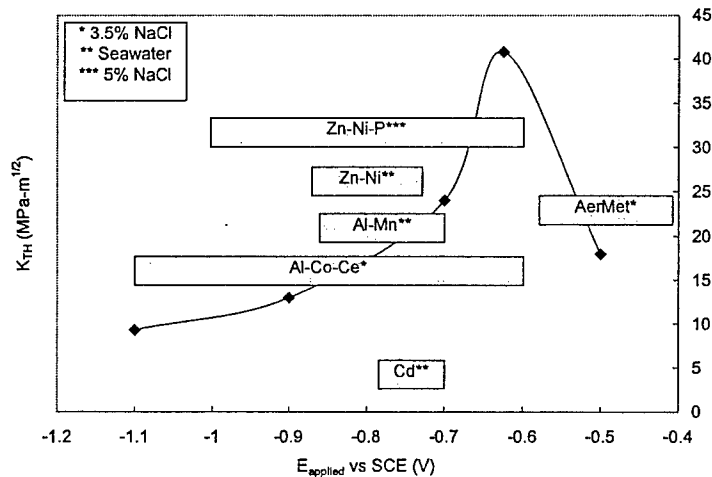

Figure 6. K_{TH} versus $E_{applied}$ for AERMET 100 in 3.5% NaCl. Open circuit potential ranges are also shown for various candidate coatings in NaCl electrolytes.
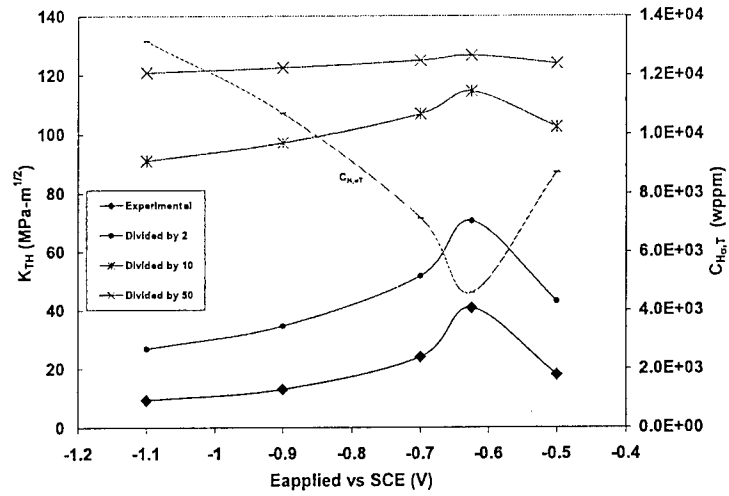
Figure 7. Predicted (dotted lines) and experimental (◆) K_{TH} versus $E_{applied}$ for varying values of $C_{lattice}$. The plotted $C_{lattice}$ values were calculated from experimental K_{TH} data. Predicted values of K_{TH} were determined using calculated $C_{lattice}$ values divided by 2, 10, and 50. A hydrostatic stress field, σ_H, of $5\sigma_{ys}$ is assumed.